The Balance of Thermodynamic Potentials in Solar Cells Investigated by Numerical Device Simulations

Felix Komoll and Uwe Rau

***Abstract*—This article presents an extension of the classical gain/loss analysis of Brendel et al. based on the balance of free energy in a solar cell. We consider the full balance of all thermodynamic potentials by separating the excess free energy into excess chemical and excess electrostatic potentials. A layer-by-layer analysis of an exemplary silicon solar cell shows that the different functionalities of different parts of the solar cell, e.g., the neutral base and the space charge regions, are well reflected in the different pictures provided by looking at the thermodynamic potentials separately. Additionally, we investigate fill factor losses by insufficient majority carrier collection at the back contact of the solar cell with two prototypical passivation layers. Here we show that resistive losses, i.e., losses in the electrostatic potential can be distinguished from kinetic losses, i.e., losses in the chemical potential.**

***Index Terms*—Free energy flux, gain/loss analysis, numerical simulation, thermodynamic potentials.**

I. Introduction

A SOLAR cell transforms radiation energy from the sun into electrical energy at the cell's terminals. The photovoltaic effect that takes place within the solar cell consists of two separate steps: First, the continuous generation of electron/hole pairs, i.e., the generation of fluxes of excess chemical potentials and, second, the transformation of this chemical energy flux into electrical power, i.e., the product of electrical current and voltage at the cell's terminals. Since, the electrochemical potentials $\eta_{n,p}$ of electrons and holes are the respective sum of their chemical potentials $\mu_{n,p}$ and their electrical potentials $\varphi_{n,p}$, the analysis of gains and losses in solar cells is conveniently made in terms of the overall electrochemical potential $\eta = \eta_n + \eta_p$[1]. However, summarizing two different thermodynamic potentials, the chemical and the electrostatic potentials, into one hides a part of the photovoltaic action of the solar cell, namely the transformation of chemical energy into electrical energy.

Therefore, we propose here a more complete thermodynamic gain/loss analysis that extends the previous approach of Brendel et al. [1] by separating the free energy balance into the balance of chemical and electrostatic potentials. We use data from numerical device simulations (SCAPS [2]) to illustrate our method for the example of a generic silicon pn-junction solar cell with selective contacts. The theory behind our approach is delineated in Section II and the settings of the simulations in Section III. Finally, an exemplary layer by layer functional analysis of the solar cell highlights the different roles played by the neutral base of the solar cell and the space charge regions (SCRs) at the *pn*-junction and at the high/low-junction (see Section IV-A).

Finally, we apply our method to two paradigmatic variations of the passivation layer at the high-low junction (back contact of the solar cell). These two variations are chosen to find examples for two distinct approaches to contact selectivity, namely the resistive model by Brendel and Peibst [3], and the kinetic model by Roe et al. [4]. As discussed in [5], these models are not compatible. Rather they describe specific situations where the losses show up as losses in the electrostatic potential (resistive) or chemical potential (kinetic), exclusively. Thus, the present analysis method should be able to bridge this gap by considering the electrostatic and the chemical potential losses individually (see Section IV-B).

II. Theory

Let us consider the excess electrostatic potential of electrons via $\delta\varphi_n = -q\delta\Phi$ (in units of electron volts) such that the excess free energy of electrons $\delta\eta_n$ is given by

$$\delta\eta_n = \delta\mu_n - q\delta\Phi = \delta\mu_n + \delta\varphi_n. \tag{1}$$

With the same line of arguments

$$\delta\eta_p = \delta\mu_p + q\delta\Phi = \delta\mu_p + \delta\varphi_p \tag{2}$$

holds for the excess free energy of holes. The flux p_{free} of the free energy may be looked at as the sum of fluxes p_{elec} and p_{chem} of electrostatic energy and chemical energy. From the particle current densities j_n and j_p we obtain finally

$$\begin{aligned} p_{\text{free}} &= j_n\,\delta\eta_n + j_p\,\delta\eta_p = j_n\,(\delta\mu_n + \delta\varphi_n) + j_p\,(\delta\mu_p + \delta\varphi_p) \\ &= (j_n - j_p)\,\delta\varphi_n + j_n\delta\mu_n + j_p\delta\,\mu_p = p_{\text{elec}} + p_{\text{chem}}. \end{aligned} \tag{3}$$

This equation is now used as the base for the analysis of the balance of the three thermodynamic potentials (x = free, elec, chem) in each layer and at across each interface in the solar cell according to

$$\Delta\, p_x^k = p_x^{k,\text{out}} - p_x^{k,\text{in}} \tag{4}$$

Manuscript received 30 May 2022; revised 10 August 2022; accepted 11 August 2022. Date of publication 8 November 2022; date of current version 28 November 2022. This work was supported by the German Federal Ministry of Economic Affairs and Climate Action (BMBK) under Contract 0324353B ('CIGSTheoMax'). *(Corresponding author: Felix Komoll.)*

The authors are with the IEK-5 Photovoltaik, Forschungszentrum Jülich GmbH, 52425 Jülich, Germany and also with the Faculty of Electrical Engineering and Information Technology, RWTH Aachen University, 52074 Aachen, Germany (e-mail: f.komoll@fz-juelich.de; u.rau@fz-juelich.de).

Color versions of one or more figures in this article are available at https://doi.org/10.1109/JPHOTOV.2022.3207600.

Digital Object Identifier 10.1109/JPHOTOV.2022.3207600

where the index k denotes the number of a specific layer or of a specific interface.

For the chemical potential, we can distinguish a component resulting from the generation and recombination of electron hole pairs and a component from kinetic transport losses due the finite mobility of the charge carriers. The balance of chemical potential of electrons reads

$$\begin{aligned}\Delta\, p^k_{\mathrm{chem},n} &= j_n^{k,\mathrm{out}}\,\delta\mu_n^{k,\mathrm{out}} - j_n^{k,\mathrm{in}}\delta\mu_n^{k,\mathrm{in}} \\ &= \frac{\delta\mu_n^{k,\mathrm{out}}+\delta\mu_n^{k,\mathrm{in}}}{2}\left(j_n^{k,\mathrm{out}}-j_n^{k,\mathrm{in}}\right)+\frac{j_n^{k,\mathrm{out}}+j_n^{k,\mathrm{in}}}{2} \\ &\quad \left(\delta\mu_n^{k,\mathrm{out}}-\delta\mu_n^{k,\mathrm{in}}\right) = \Delta p^k_{gr,n}+\Delta p^k_{kin,n} \qquad (5)\end{aligned}$$

where we use the arithmetic averages of the current density and of the chemical potential such that the same equation can be applied for interfaces and for layers of finite thickness. Adding up the terms for electrons from (5) with the corresponding expression for holes yields

$$\begin{aligned}\Delta\, p^k_{\mathrm{chem}} &= \Delta p^k_{gr,n}\ +\Delta p^k_{gr,p}+\Delta p^k_{\mathrm{kin},n} \\ &\quad +\Delta\, p^k_{\mathrm{kin},p} = \Delta p^k_{gr}\ +\Delta p^k_{\mathrm{kin}}. \qquad (6)\end{aligned}$$

Note that the difference between outgoing and ingoing electron current density equals the difference in hole current densities and both quantities correspond also to the difference between the generation current $j_g$and the recombination current j_r according to

$$\left(j_n^{k,\mathrm{out}}-j_n^{k,\mathrm{in}}\right)=\left(j_p^{k,\mathrm{out}}-j_p^{k,\mathrm{in}}\right)\ =j_g\ -j_r. \qquad (7)$$

Finally, because $\delta\ \varphi_n = \ -\delta\varphi_p$, we may write for the balance of the chemical potential by generation and recombination within a layer k

$$\begin{aligned}\Delta\, p^k_{gr} &= \frac{\delta\mu_n^{k,\mathrm{out}}+\delta\mu_n^{k,\mathrm{in}}+\delta\mu_p^{k,\mathrm{out}}+\delta\mu_p^{k,\mathrm{in}}}{2}\ (j_g-j_r) \\ &= \frac{\delta\eta_n^{k,\mathrm{out}}+\delta\eta_n^{k,\mathrm{in}}+\delta\eta_p^{k,\mathrm{out}}+\delta\eta_p^{k,\mathrm{in}}}{2}\ (j_g-j_r)\,. \qquad (8)\end{aligned}$$

Equation (8) implies that the first step of the photovoltaic effect, namely the generation of excess electron hole pairs (considering j_g only), can be looked at as a generation of free energy, but equally as the generation of chemical energy.

III. Simulation Details

The prototype silicon solar cell structure considered in this article is a silicon solar cell containing two generic selective contacts. The present article concentrates on the majority carrier collection at the back contact with two variations of the type of the passivation layer ('thick" and "thin" as shown by item 2 of the list below).

The solar cell is defined by the following layers in order from back to front side:

1) A 0.1 μm thick p+ Si back contact layer (acceptor density: 2.8×10^{19} cm^{-3}, electron/hole mobility: $4.5\times10^3/1.5\times10^3$ cm^2/(Vs)).
2) The "thick" variant of the passivation layer has a thickness of 1 μm [acceptor density: 2.8×10^{19} cm^{-3}, electron/hole mobility: $2\times10^{-2}/1\times10^2$ cm^2/(Vs)]. The conduction band of this layer is set 0.1 eV higher than the conduction band energy of the Si contact and absorber layers, accordingly the valence band is set 0.1 eV lower than valence band of the Si layer. Variations for the majority carrier (hole) collection with respect to the reference are achieved by lowering the hole mobility. The "thin" variant is a 4 nm thick passivation layer [acceptor density: 2.8×10^{19} cm^{-3}, electron/hole mobility: $1\times10^1/1\times10^1$ cm^2/(Vs)]. The conduction band of this layer is set 0.4 eV higher than the conduction band energy of the Si contact and absorber layers, accordingly the valence band is set 0.1 eV lower than valence band of the Si layer for the reference and variations are achieved increasing the valence band offset as illustrated in Fig. 1.
3) A 200 μm thick p-type c-Si absorber [acceptor density: 2.8×10^{19}cm^{-3}, electron/hole mobility: $4.5\times10^3/1.5\times10^3$ cm^2/(Vs)].
4) A 0.02 μm thick generic n-passivation layer [acceptor density: 2.8×10^{19} cm^{-3}, electron/hole mobility: $4.5\times10^2/1.5\times10^3$ cm^2/(Vs)]. The conduction and valence band energies are the same as in the passivation layer (2). Variations of the passivation layer at the n-side of the solar cell are not considered in this article.
5) A 0.1 μm n+-Si layer [acceptor density: 2.8×10^{19} cm^{-3}, electron/hole mobility: $4.5\times10^3/1.5\times10^3$ cm^2/(Vs)].

Except for the passivation layers, the cell is defined on base of the standard silicon settings in the numerical device simulation SCAPS [2].

A batch simulation is used to compute a series of band diagrams of the solar cell for a series of voltage bias points. For

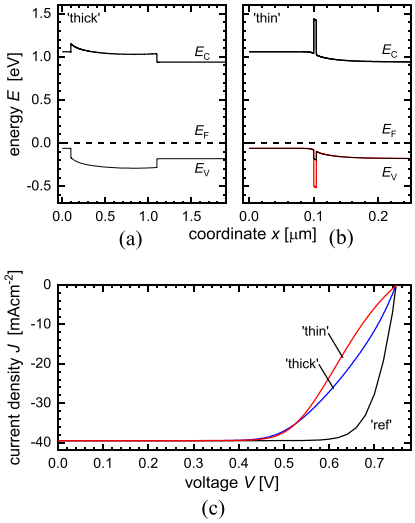

Fig. 1. (a) Equilibrium band diagram for a $p/p+$ junction in a silicon solar cell featuring a generic 1μm thick passivation layer. (b) Equilibrium band diagram for a junction with a 4 nm thin passivation layer with two different valence band offsets (0.1 eV, black, and 0.42 eV, red) with otherwise unchanged parameters. Variations are made to the hole mobility in the thick layer and in the band offset for the thin layer in order to vary the junctions' ability to collect holes. (c) Current voltage characteristics of a reference calculation for thin and thick passivation layers with favorable mobilities and band offsets leads in both cases to the same current-voltage characteristics. A reduction of the hole mobility from 100 s to 0.7 cm^2/Vs for the thick passivation layer and an increase of the valence band offset from 0.1 to 0.42 eV leads to the two characteristics with reduced fill factor.

this article, the applied bias voltage ($V_{\rm bias}$) starts at 0 mV and is linearly increased in 37 mV increments until $V_{\rm bias} = 748$ mV $= V_{\rm oc}$ arrives at the open-circuit voltage. The maximum power point (MPP) of the device is reached at a voltage of $V_{\rm bias} =$ 630 mV.

Simulations are conducted in the dark and under illuminated conditions to cover the equilibrium and the nonequilibrium situation. The illumination is set to the standard AM1.5G spectrum which is included in the software. Further, the recorder function in SCAPS is utilized to gather data of the following six quantities: conduction and valence band energies $E_C(x)$ and $E_V(x)$, the quasi-Fermi energies $E_{Fn}(x)$, $E_{Fp}(x)$ for electrons and holes, as well as the electron and hole currents $j_n(x)$ and $j_p(x)$. Only these six quantities are needed as the basis for the following analysis of the full balance of thermodynamic potentials. The layer-by-layer analysis uses the five layers above, moreover, considers the SCRs at the *pn*-junction and at the high/low junction as additional layers, as well as all interfaces between the layers and from the first and last layer to the metallic contact.

Fig. 1(a) shows the equilibrium band diagram of the solar cell in the vicinity of the "thick" passivation layer. Here. the variations in the majority collection are achieved by reducing the hole mobility in the layer without altering the band diagram. Fig. 1(b) shows the reference band diagram for the "thin" passivation layer with a valence band offset of 0.1 and of 0.42 eV (red line). The latter variation is made to investigate the effect of a large barrier on the collection of holes.

Fig. 1(c) shows the four current voltage (*IV*) characteristics of the two reference systems (thick passivation layer with high hole mobility, thin passivation layer with low valence band offset). The *IV* curves of the two reference cells are identical featuring a high open circuit voltage of 748 mV, a short circuit current density of 39.5 mAcm^{-2}, and a fill factor of 82.0%. In contrast the reduction of carrier mobility, by either lower hole mobility in the "thick" passivation layer or by a higher valence band offset for the 'thin' layer, lead to a significant reduction of the fill factor to 62.8% and 63.5%, respectively. These two situations are designed with the goal to find examples where the fill factor losses follow the resistive model of Brendel and Peibst [3], i.e., the free energy losses result from losses in the electrostatic potential or the kinetic model of Roe et al. [4], i.e., free energy losses are losses in the chemical potential.

IV. Results

A. Balance of Thermodynamic Potentials for the Reference Cell

Fig. 2 shows the band diagram of the reference Si-solar cell (with the 'thick' passivation layer) under illumination and at a voltage corresponding to the MPP $V_{\rm bias} = 630$ mV. Note that the passivation layers are assumed to have high mobilities for the respective majority carriers, i.e., the carriers that should be extracted at the specific contact, and low mobilities for the respective other carriers. Furthermore, no interface recombination is assumed, such that the contacts can be considered almost perfectly selective [3], [4], [5] and the Si absorber material dominates the carrier recombination in the cell. Thus, we start with the most generic and simple situation for a *pn*-junction solar cell.

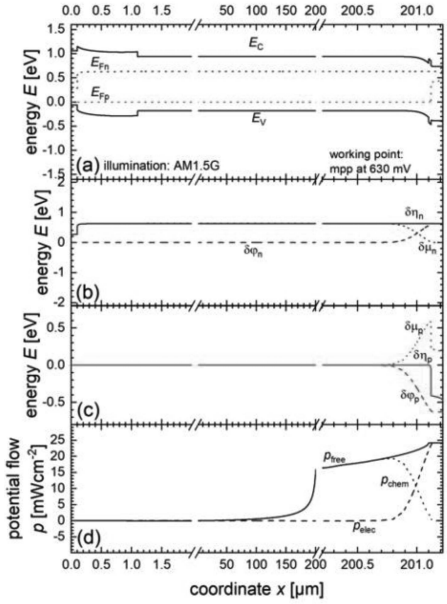

Fig. 2. (a) Nonequilibrium band diagram of a silicon solar cell under AM1.5G illumination and at $V_{\rm mmp}$. The cell has two generic passivation layers between the highly *n*- and *p*-doped contact layers and the moderately *p*-doped Si absorber. (b) Nonequilibrium thermodynamic potentials $\delta\eta_n$, $\delta\mu_n$, and $\delta\varphi_n$ for electrons and (c) $\delta\eta_p$, $\delta\mu_p$, and $\delta\varphi_p$ for holes. (d) Fluxes $p_{\rm free}$, $p_{\rm elec}$, and $p_{\rm chem}$ of the electrochemical, the electrostatic, and the chemical potential.

Fig. 2(b) and (c) shows the nonequilibrium potentials $\delta\eta_n$, $\delta\mu_n$, and $\delta\varphi_n$ for electrons and $\delta\eta_p$, $\delta\mu_p$, and $\delta\varphi_p$ for holes, respectively. The most important observation in Fig. 2(b) is that the chemical potential $\delta\mu_n$ of electrons decreases from the neutral part of the Si-absorber (where a major part of $\delta\mu_n$ is produced by the photogeneration of excess electrons) through the SCR (coordinate $x \approx 200.7 - 201.1$ μm) toward the electron contact. At the same time the electrostatic potential $\delta\varphi_n$ increases by the same amount, such that the electrochemical potential $\delta\eta_n$ remains constant. This transformation of excess chemical potential in the absorber into electrical potential at the contact is the essence of the photovoltaic effect procured by an active junction in a solar cell. Note that the same transformation takes place also for $\delta\mu_p$ and $\delta\varphi_p$ in Fig. 2(c).

Finally, it can be seen in Fig. 2(b) and (c) that across the passivation layers the electrochemical potential as well as the chemical potential of the respective minority carriers is reduced from high values in the absorber to low values in the highly doped contact layers.

Fig. 2(d) compares the fluxes $p_{\rm free}$, $p_{\rm elec}$, and $p_{\rm chem}$ of the three thermodynamic potentials (3) at the given working point. At the left terminal ($x = 0$) all three potentials are zero, whereas at the right terminal ($x = 201.22$ μm) the electrical as well as the electrochemical potential flux correspond to the extracted power of 24.17 mWcm^{-2}. The chemical potentials and in consequence the flux of chemical potentials is at this point zero as it should be at a metallic terminal of the solar cell. It is also seen in Fig. 2(d) that the electrostatic power $p_{\rm elec}$ is built up exclusively in the SCRs of the *pn*-junction and of the high-low junction. The

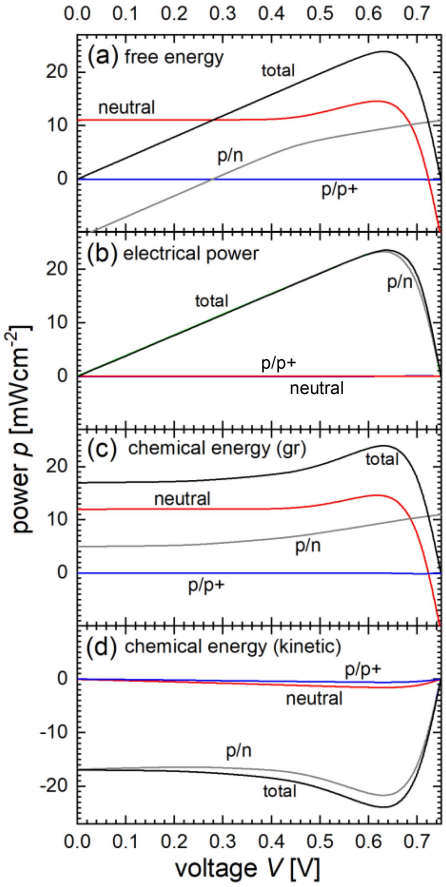

Fig. 3. Contributions of the different layers to (a) the free energy (electrochemical potential) flux. (b) Flux of the electrostatic potential (electrical power), (c) Flux of the chemical potential (contribution of generation and recombination). (d) Kinetic part of the chemical potential flux, according to (4) and (5). Note that the seven layers in the device are divided into three groups: The *n*/*n*+-junction, the neutral part of the Si absorber, and the *p*/*p*+-junction.

electrochemical potential flux p_{free} builds up in the SCR of the pn-junction as well as in the neutral absorber. Especially outside the SCR, p_{free} follows closely p_{chem}.

Fig. 3 illustrates the layer by layer analysis of the contributions Δp^k_{free}, Δp^k_{elec}, Δp^k_{gr}, and Δp^k_{kin} of the different layers to the free energy flux, the electrical power and the two components of the chemical energy flux as defined in (5) and (6) calculated for the voltage bias points between zero and $V = V_{\text{oc}} = 745$ mV. Note that for the sake of simplicity, the seven layers are combined into three groups of layers, namely the neutral part of the absorber, the *n*/*n*+-junction (including the SCR of the *p*/*n*-junction, the *n*-passivation layer and the highly doped *n*+ contact layer) and the *p*/*p*+-junction (comprised of the SCR of the high/low-junction, the p-passivation layer and the highly doped *p*+ contact layer).

Free energy fluxes [see Fig. 3(a)] are only present in the neutral part of the absorber and in the *p*/*n*-junction. For the contribution of the neutral part, we have to understand that below a voltage of 350 mV, the split of the Fermi-levels in the illuminated absorber does not correspond to the external voltage. This is because at zero or low external voltage a certain amount of free energy is needed to drive the minority carriers (electrons) from the absorber through the SCR into the contact [6], [7]. In this situation, photogeneration leads to the generation of free energy in the absorber, which is however immediately consumed in the *p*/*n*-junction, such that the sum of both potentials is always the externally extracted power. At higher voltages the free energy generation increases up to a point where the annihilation of free energy by recombination in the neutral absorber prevails and finally defines the open circuit situation. The electrostatic picture [see Fig. 3(b)] shows that the transformation of chemical into electrical energy takes place only in the *p*/*n*-junction.

Fig. 3(c) demonstrates that the photogeneration in the neutral absorber and in the *p*/*n*-junction are the main contributors to the generation of chemical energy due to the photogeneration of charge carriers in these two regions. Finally, Fig. 3(d) shows the kinetic part of the chemical energy. All contributions are negative because they either consume chemical energy due to (quasi-) resistive losses or they transform chemical energy into electrical energy which also yields a negative contribution to the chemical energy. Note that the sum of the contributions Δp^k_{gr} and Δp^k_{kin} over all layers must yield zero chemical energy at all bias points [see Fig. 2(d)].

B. Loss Analysis at Reduced Selectivity of the High/Low Junction

After having illustrated the basic working principle of a solar cell in the light of its balance of thermodynamic potentials, we use the same tool to investigate the losses that are caused by the deterioration of the majority carrier collection efficiency for the two paradigmatic passivation layers at the high/low junction. As discussed above, for the 'thick' layer this is achieved by reducing the hole mobility μ_h from 100 cm^2/Vs (reference) to 0.7 cm^2/Vs. In Fig. 4(a), we show the free energy balance for the device with reduced hole mobility with a considerable loss at the *p*/*p*+ junction. This loss leads to the fact that the free energy generated in the device (black line) is lower than the sum of the free energies generated in the absorber (red) and in the SCR region (green) of the *p*/*n*-junction. The electrical picture in Fig. 4(b) reflects the loss in the *p*/*p*+ contact as a negative contribution counterbalancing the electrostatic potential that is generated by the *p*/*n*-junction. A closer look at the electrical balance of the three involved layers [see Fig. 4(c)] unveils that the loss of the electrical energy occurs essentially over the thick passivation layer. Fig. 4(d) shows the kinetic part of the chemical energy for the absorber and the junctions. Here, we concentrate on the fact that there is no kinetic loss in the *p*/*p*+-junction except for higher voltages (blue line). However, looking at the details of the kinetic flux balance of the *p*/*p*+ junction in Fig. 4(e), i.e., to the contributions of the three constituting layers, we find that the apparent zero balance of the junction at voltages < 0.6 V is composed of the accumulation of chemical energy in the SCR and a loss of chemical energy in the passivation layer.

Fig. 5(a) shows the non-equilibrium band diagram zoomed in to the region of the *p*/*p*+ junction and Fig. 5(b) the excess potentials $\delta\eta_p$, $\delta\mu_p$, and $\delta\varphi_p$ for the holes, which are of interest here. We can readily see that the free energy and the electrostatic potential roughly follow each other. Analogously, the flux of the free energy and the flux of electrical energy displayed in Fig. 5(c) follow each other. However, small discrepancies between those potentials [see Fig. 5(b)] as well as between the fluxes occur at

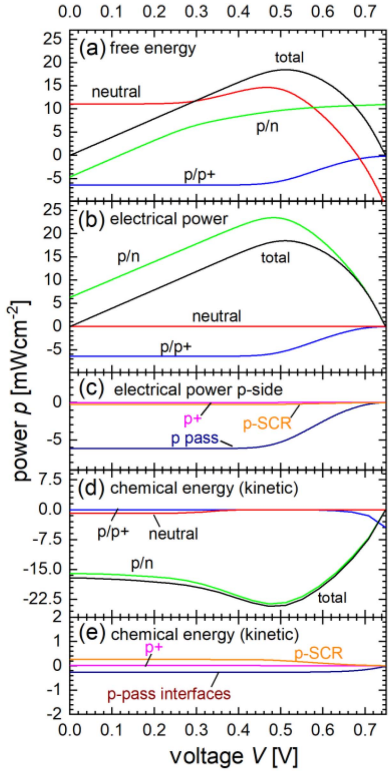

Fig. 4. (a) Free energy (electrochemical potential) flux for the solar cell with a 'thick' passivation layer and the hole mobility in this layer reduced to $\mu_h = 0.7$ cm^2/Vs. The black line is the total free energy flux extracted from the device. The layer-by-layer analysis shows the free energy extracted from the neutral absorber (red), the p/n-junction (including the SCR, the passivation layer, and the $n+$-doped contact layer, green), and from the p/p+ junction (including the SCR, the passivation layer, and the $p+$-doped contact layer, blue). (b) Flux of the electrostatic potential (electrical power) of the three layers, featuring a negative contribution from the $p/p+$ junction due to the low hole mobility in the passivation layer. (c) Electrostatic flux balance of the $p/p+$ junction detailed to the contributions of the three constituting layers SCR, passivation layer and $p+$-doped contact layer, featuring the fact the electrical power is lost over passivation layer. (d) Kinetic part of the chemical energy for the absorber and the junctions, featuring a transport loss in the absorber at lower voltages and no kinetic losses in the $p/p+$-junction except for higher voltages. (e) Kinetic flux balance of the p/p+ junction detailed to the contributions of the three constituting layers. Here it is shown that the zero balance of the junction at voltages < 0.6 V is composed of the accumulation of chemical energy in the SCR that is consumed in the passivation layer.

either side of passivation layer leading to a chemical potential that is slightly above zero (accumulation of holes) to the right and slightly below zero (depletion of holes) at the left side of the layer [dotted line in Fig. 5(b)]. What we observe here is essentially the charging of the capacitor across the passivation layer that is necessary to build up the excess electrical field that drives the holes through the passivation layer. Thus, the present "thick" layer turns out to be a good example for a purely resistive loss across the passivation layer.

In the next step, we discuss the reduced ability for majority collection through the 'thin' passivation layer. This is achieved by increasing the valence band offset from 0.1 eV (reference) to 0.42 eV. In Fig. 6(a), we show the free energy balance for this device displaying a loss at the $p/p+$ junction (blue line) much as in the case of the "thick" layer with reduced hole mobility. The

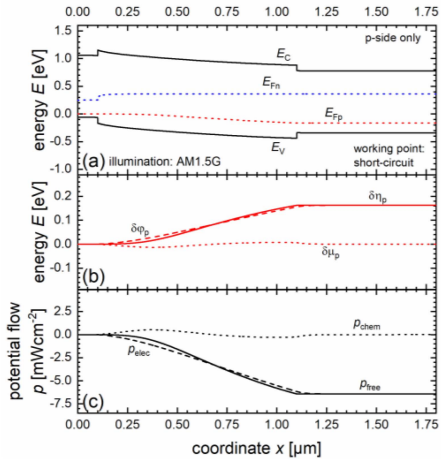

Fig. 5. (a) Nonequilibrium band diagram under illumination and short circuit for the p/p+ junction region of the solar cell with a 'thick' passivation layer and the hole mobility in this layer reduced to $\mu_h = 0.7$ cm^2/Vs. (b) Nonequilibrium thermodynamic potentials $\delta\eta_p$, $\delta\mu_p$, and $\delta\varphi_p$ for holes, featuring the fact that the electrostatic potential follows the free energy whereas the chemical energy remains essentially unchanged. (c) Fluxes p_{free}, p_{elec} , and p_{chem} of the electrochemical, the electrostatic, and the chemical potential. The free energy flux (loss) and the electrostatic energy flux follow closely each other. This is a good example of a purely resistive loss across the passivation layer.

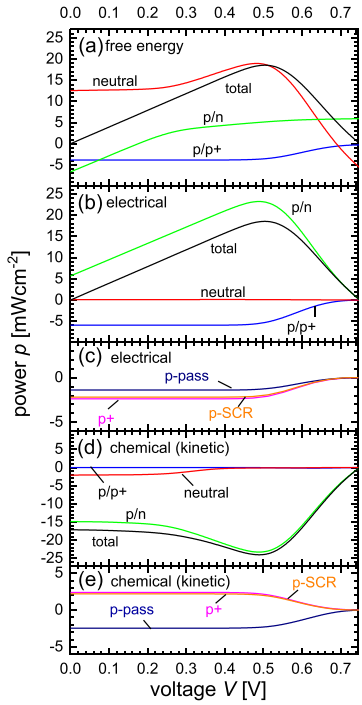

Fig. 6. (a) Free energy (electrochemical potential) flux for the solar cell with a 'thin' passivation layer and the valence band offset enhanced to 0.42 eV. The black line is the total free energy flux. The free energy extracted from the neutral absorber is shown in red, the p/n-junction (SCR, passivation layer, and $n+$-doped contact layer) in green, and the $p/p+$ junction (SCR, passivation layer, and $p+$-doped contact layer) in blue. (b) Flux of the electrostatic potential of the three layers, featuring negative contributions from the p/p+ junction much like in Fig. 4(b). (c) Electrostatic flux balance of the $p/p+$ junction detailed to the contributions of the three constituting layers SCR, passivation layer, and $p+$-doped contact layer, featuring contributions from all three layers to the loss of electrical power. (d) Kinetic part of the chemical energy for the absorber and the junctions. (e) Splitting in the kinetic chemical energy at voltages < 0.6 V results from an accumulation of chemical energy in the SCR and the consumption of an equal amount in the passivation layer. This in fact is the electrical power loss over the passivation layer.

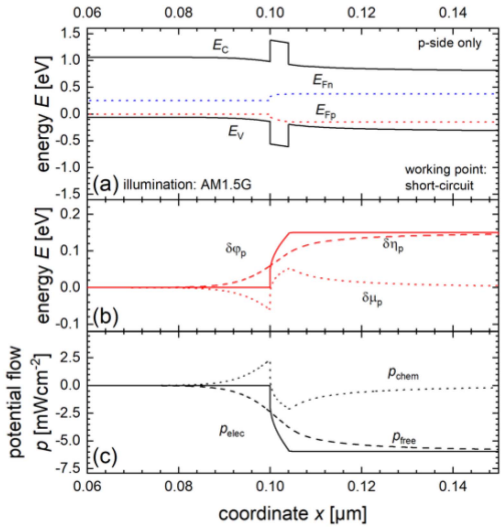

Fig. 7. (a) Nonequilibrium band diagram under illumination and short circuit for the $p/p+$ junction region of the solar cell with a 'thin' passivation layer (valence band offset enhanced to 0.42 eV). Note the higher spatial resolution as compared to Fig. 5. (b) Nonequilibrium thermodynamic potentials $\delta\eta_p$, $\delta\mu_p$, and $\delta\varphi_p$ for holes. Outside the immediate junction volume, the electrostatic potential equals the free energy. Close to the absorber/passivation layer interface, the enhanced chemical potential results from accumulation on the right side and a depletion of holes on the left side of the interface. (c) Fluxes p_{free}, p_{elec} , and p_{chem} of the electrochemical, the electrostatic, and the chemical potential. The free energy flux (loss) and the electrostatic energy flux follow each other only outside the immediate junction volume.

electrical picture in Fig. 6(b) is also very similar to Fig. 4(b), especially as far as the loss in the $p/p+$ contact shows up in the electrical potential and there is no loss in chemical potential across the junction in Fig. 6(d). Separating the contributions of the three individual layers in Fig. 6(c) (SCR, passivation layer, $p+$ doped layer) shows that the electrical loss occurs over all three layers with the passivation layer having the smallest contribution due to its low thickness of only 4 nm. The flux of chemical potential shown in Fig. 6(e) shows positive balances for the p+-layer and for the SCR of the absorber layer compensated by a negative balance for the passivation layer such that the overall consumption of chemical energy is zero [see Fig. 6(d)].

The nonequilibrium band diagram of the junction region for the "thin" passivation layer is shown in Fig. 7(a) and the excess potentials $\delta\eta_p$, $\delta\mu_p$, and $\delta\varphi_p$ for the holes in Fig. 7(b), both in high spatial resolution. In Fig. 7(b), we see that the free energy of holes drops sharply over the passivation layer due to the high barrier that the holes have to overcome. We see an equivalent drop of the chemical potential over this layer. Hence, we have *locally* a loss in chemical potential. However, we see also that the chemical potential gets back to zero after a short distance to the left and to the right of the passivation layer such that there is no difference between the free energy and the electrostatic potential. Thus, *globally* the loss of free energy across the entire p/p+ junction is resistive. The flux of thermodynamic potentials displayed in Fig. 7(c) displays the analogous picture.

Again, we may consider the picture of a capacitor across the passivation layer (which is much narrower here than at the "thick" layer): Holes accumulate and deplete close to the transport obstacle, i.e., the passivation layer. And although there is a loss in chemical energy across the thin passivation layer, the overall picture is that the chemical energy is merely shifted forth and back with an overall loss of zero.

V. Summary

The present article has highlighted the interplay between chemical, electrochemical, and electrostatic potential in a solar cell. We have used numerical simulations of a rather ideal silicon *pn*-junction solar cell to illustrate and quantify the fluxes of the three different potentials in this generic case. We have shown that the generation of chemical potential (i.e., excess electrons and holes) takes place in the absorber and the SCR of the pn-junction, whereas the transformation of this chemical energy into useful electrical energy available at the cell's terminals is achieved essentially within the SCR of the *pn*-junction. A detailed loss analysis for two generic passivation layers at the $p/p+$ back junction unveiled that a thick passivation layer with relatively low hole mobility exhibits losses exclusively in the electrostatic potential. This situation would be perfectly covered by the selectivity model of Brendel and Peibst [3]. A thin passivation layer with a high band offset for holes shows a more complex picture: Across the thin layer itself both, free energy as well as chemical energy is lost. However, the chemical energy loss is perfectly counterbalanced by accumulation of chemical energy in the absorber and in the highly doped contact in the vicinity of the passivation layer. Thus, globally the loss across the entire high/low junction is also resistive, i.e., it can be described by a voltage drop across the junction, again as in the model of [3]. We, thus, conclude that for a high-low junction where the critical layer is packed between two doped layers of equal polarity, the losses are mostly resistive. We finally note that this behavior of a high-low junction is, however, in sharp contrast to free energy losses across or within pn-junctions that are clearly kinetic as described elsewhere [8].

Acknowledgment

The authors would like to thank T. Kirchartz and M. Riencker for discussions.

References

[1] R. Brendel, S. Dreissigacker, N. P. Harder, and P. Altermatt, "Theory of analyzing free energy losses in solar cells," *Appl. Phys. Lett.*, vol. 93, 2008, Art. no. 173503.
[2] M. Burgelman, P. Nollet, and S. Degrave, "Modelling polycrystalline semiconductor solar cells," *Thin Solid Films*, vol. 527, pp. 361–362, 2000.
[3] R. Brendel and R. Peibst, "Contact selectivity and efficiency in crystalline silicon photovoltaics," *IEEE J. Photovolt.*, vol. 6, no. 6, pp. 1413–1420, Nov. 2016.
[4] E. T. Roe, K. E. Egelhofer, and M. C. Lonergan, "Limits of contact selectivity/recombination on the open-circuit voltage of a photovoltaic," *ACS Appl. Energy Mater.*, vol. 1, 2018, Art. no. 1037.
[5] U. Rau and T. Kirchartz, "Charge carrier collection and contact selectivity in solar cells," *Adv. Mater. Interfaces*, vol. 6, 2019, Art. no. 1900252.
[6] O. Breitenstein, "An alternative one-diode model for illuminated solar cells," *IEEE J. Photovolt.*, vol. 4, no. 3, pp. 899–905, May 2014.
[7] U. Rau, V. Huhn, and B. E. Pieters, "Luminescence analysis of charge-carrier separation and internal series-resistance losses in Cu(In,Ga)Se_2 solar cells," *Phys. Rev. Appl.*, vol. 14, 2020, Art. no. 014046.
[8] U. Rau, unpublished.